Control of the Plasma-Material Interface for Long Pulse Optimization in EAST - Final Report

Lead Principle Investigator: R. Maingi, Princeton Plasma Physics Laboratory

Institutional PI: K. Tritz, Johns Hopkins University

Institutional PI: J Canik, Oak Ridge National Laboratory

Institutional PI: B. Wirth, University of Tennessee at Knoxville

Institutional PI: D. Andruczyk, University of Illinois at Urbana-Champaign

Institutional PI: K. Woller, Massachusetts Institute of Technology

Institutional PI: Z. Wang, Los Alamos National Laboratory

1.0 Introduction and Background

Low-z impurities are injected into magnetic fusion devices to improve plasma performance, e.g. wall conditioning¹, control of edge-localized modes (ELMs)², and enhancement of power and particle exhaust. In this topic, we propose to continue experiments that inject a range of impurities for wall conditioning, plasma-material interactions, and plasma performance enhancement studies. The use of low-z impurities to improve performance is discussed in this sub-section, while technical details of the actuators: the impurity powder dropper (IPD)³, the impurity granule injector (IGI)^{4, 5}, and flowing liquid lithium limiters (FLiLi)⁶, are discussed in the Methods sub-section.

Wall conditioning and performance enhancement, ELM suppression

One of the first demonstrations of the benefits of low-z coatings was the use of gaseous boronization applied before a campaign to enable access to quiescent, very high confinement, or VH-mode discharges⁷. Well-established, gaseous boronization nevertheless entails handling hazardous gases (e.g. B_2D_6), which usually require interruption of experimental operation and evacuation of the facility. More recently preconditioning of the walls with inter-discharge Li evaporation allowed systematic recycling reduction and confinement improvement^{8, 9}, and elimination of ELMs^{10, 11}. However gaseous and evaporative impurity choices are limited; injection of solid materials opens up a range of usable materials. Moreover, inter-discharge conditioning procedures are inapplicable to long-pulse devices, where coatings are expected to erode significantly during a single discharge. Thus, we highlight examples of solid low-z real-time material injection for discharge improvement, starting with Li as the lowest Z impurity.

Li powder injection directly into H-mode discharges in NSTX¹², EAST¹³, and DIII-D¹⁴ reduced the ELM frequency and improved edge stability. Fig. 1 compares a sequence of ~ 25 sec long discharges in EAST with Li injection (red) and without (black)¹³. The baseline divertor D_{α} emission, indicative of the overall

recycling flux, was reduced by more than 50%. ELMs, which can be observed as the small 'spikes' in the D_{α} emission, were completely eliminated during the periods of Li injection, and reappeared when Li injection was terminated, e.g. #41075. These early promising studies were conducted on graphite PFCs in all three devices, and in EAST, had relatively poor normalized energy confinement (H98y2~0.75). Thus, the extrapolability of ELM elimination during Li injection with high-Z PFCs remained to be proven.

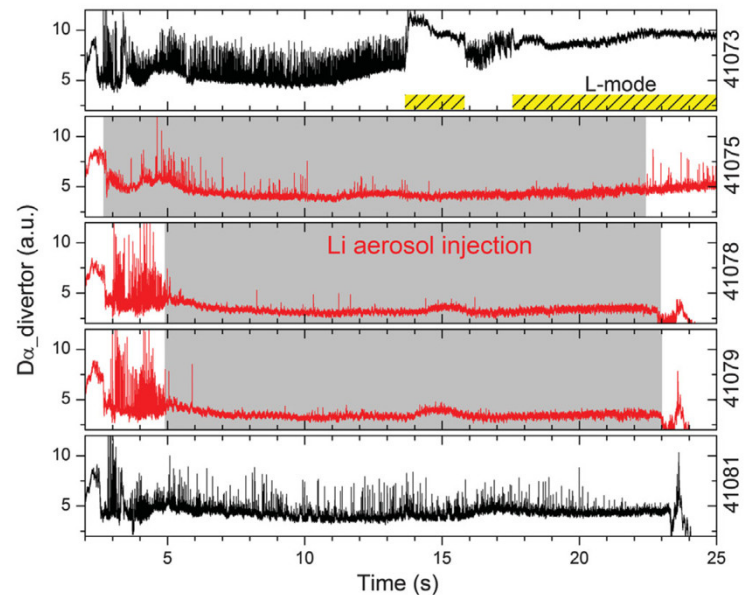


Fig. 1: D_{α} emission from a sequence of discharges with Li powder injection (red) and without (black). Li powder injection resulted in ELM suppression. [13]

Due to concerns of Li chemical reactivity and hydrogenic species retention in a reactor, most fusion devices choose to condition walls with boron instead. Experiments carried out in the DIII-D tokamak explored the possibility of generating boron coatings in "real-time", by injection of B and B enriched powders during tokamak operation. Boron injection into DIII-D H-mode plasmas (graphite PFCs) correlated with reduction of recycling and impurity concentrations during the initial plasma current ramp (Fig. 2)¹⁵. Despite higher fueling from the gas feedback system, the electron density was markedly lower

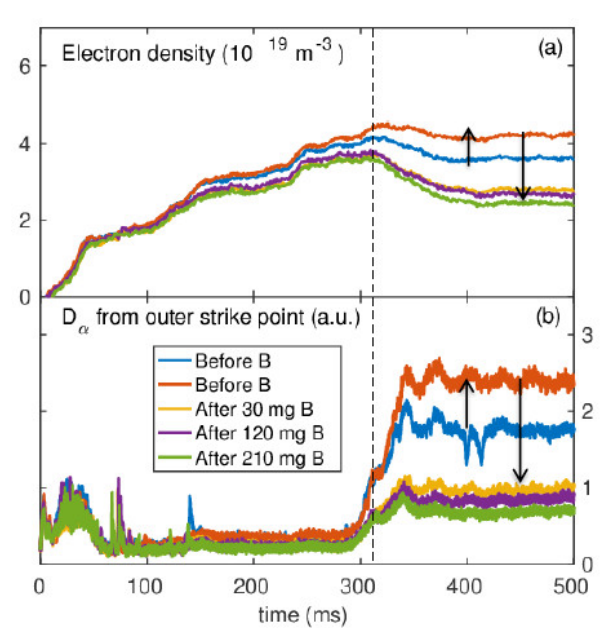


Fig. 2: (a) Discharge ramp-up electron density before (blue, orange) and after (yellow, purple, green) B conditioning, showing lower density due to reduced wall fueling [15]

in the discharges following B conditioning. These types of studies need to be extended to long pulse devices, and also those with high-Z PFCs, to determine if real-time injection could maintain good wall conditions for the duration of the pulse.

To uncover the governing physics, it is necessary to investigate powder ablation in the boundary plasma, the impurity transport in the scrape-off layer (SOL) and divertor, and the plasma-surface interactions and plasma chemistry of film generation on the PFCs. Regarding ablation, investigation of the circumstances under which powder experiences neutral gas shielding (NGS), typically above a critical individual particulate diameter, could become important, since NGS reduces ablation rates and amplifies penetration depth¹⁶.

Power exhaust enhancement

Power exhaust with acceptable heat flux to PFCs remains a strong concern for future reactors. Solid W PFCs have an accepted steady heat flux limit of 5-10 MW/m², depending on the neutron damage, and the size and frequency of ELM transients on top of the steady heat flux. Nearly all reactor designs with solid PFCs require radiated power from the divertor and edge

regions to reduce the plasma heat flux directly on the divertor. The problem is exacerbated by the experimentally-identified narrowing of the heat flux footprint with increasing midplane poloidal magnetic field¹⁷⁻¹⁹, projecting a ~ 1mm upstream SOL width in reactors, requiring even higher levels of dissipation to reduce peak heat fluxes to acceptable levels.

The preferred method to radiate away plasma power is addition of noble gases, e.g. Ne in present day devices, and Ar and Kr in future devices. However low-z gases such as N_2 seem to offer an additional benefit of confinement enhancement in metal-walled devices like AUG and JET²⁰, whereas Ne does not. N_2 injection may be problematic in future devices, however, due to the formation of tritiated volatile ammonia, which can be difficult to reprocess in the tritium plant. Thus there is interest in using other low-z impurities to augment divertor radiation.

Present day divertors typically operate with a temperature below 20 eV, in either the high recycling or partially detached state. With the use of recently developed solid impurity injection techniques, it is conceivable to use solid material injection for power exhaust. A calculation of the predicted cooling rate rates for several low-Z elements was done with a radiative-coronal model including finite impurity lifetime. For typical divertor conditions with $T_e < 20$ eV, B is predicted to be the best radiator; compounds such as BN can also be evaluated 15.

ELM mitigation via ELM pacing with impurity pellets

While ELM elimination is the preferred control method to completely obviate the periodic transient heat flux, the ability to run fully ELM suppressed cases with acceptable energy confinement and impurity control remains uncertain and therefor unproven for future devices. A backup ELM control method is ELM pacing

at rates much faster than the natural ELM frequency, while counting on a reduction of the ELM amplitude and peak heat flux with increasing driven ELM frequency. This can be done with frozen deuterium fuel pellets, or with impurity pellets. Deuterium pellets have the drawback of adding fuel and recycling while triggering ELMs, while impurity pellets face the prospect of generating dust; both options should be pursued in parallel. The focus of this proposal is on the use of impurity pellets, discussed below.

ELM triggering and pacing with a lithium granule injector (LGI) was first demonstrated on EAST⁴. ELMs were paced, but at close to the natural ELM frequency, due to the technical limits on granule injection rate (~ 50 Hz) of this first LGI design. While this was a critical proof-of-principle for ELM pacing via impurity injection, there was no expected or observed reduction of peak heat flux in this study.

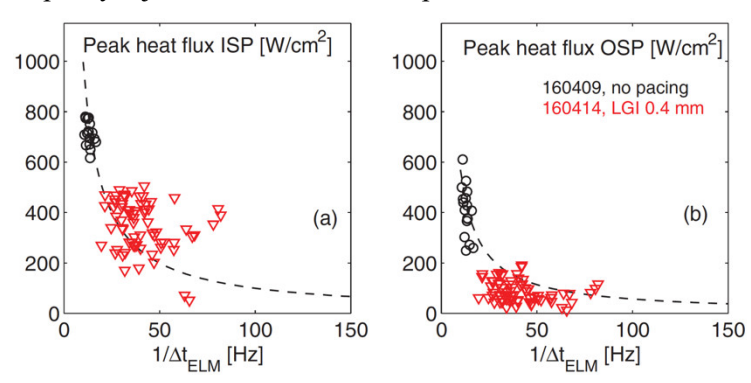


Fig. 3: peak heat flux as a function of inverse time between triggered ELMs at the inner strike point (ISP) and outer strike point (OSP) in DIII-D. [21]

An LGI capable of injecting granules at ~ 100 Hz frequency was developed and deployed on DIII-D, which can also operate with a natural ELM frequency of 10-20 Hz under certain conditions. Fig. 3 shows that the natural ELM frequency was multiplied by factors of about 5-6, with a corresponding drop of peak heat flux on the outboard side (panel (b)), but a slower drop at the inner divertor²¹. While this first result appeared promising, further experiments on DIII-D showed that the ELM size and peak heat flux could not be uniformly reduced in the ITER baseline scenario²². In that case the small ELMs augmented large ELMs, but

the large ELM frequency dropped, and the amplitude went up as collisionality was decreased. Moreover ITER needs²³ a frequency enhancement and peak heat flux reduction between 20 and 50. Thus more research is needed to assess the applicability of this technique for ITER and other future devices.

To project to future devices, it is important to characterize and model the pellet ablation physics, to determine whether the pellets deposit sufficient particles in the steep gradient region. 3D MHD modeling has indicated a critical density and pressure perturbation to trigger a 3D ballooning mode²⁴; a model benchmarked with DIII-D data for deuterium pellets was used to project the critical deuterium pellet size and speed for ELM triggering in ITER²⁵. Such a projection needs to be done for impurity pellets: the Z-dependence of the ablation physics and penetration depth needs benchmarking, as does understanding when neutral gas shielding allows deep penetration for impurity pellets, as it does for deuterium pellets. The first step, i.e. impurity pellet physics, was initiated with penetration depth measurements and modeling of the DIII-D ELM triggering with LGI²⁶, using a neutral gas shielding model for impurities with a single free parameter²⁷. The same model was applied to assess Be pellet ablation and penetration depth for ITER²⁸. The next step is to quantify the size and speed of the necessary Be pellet for ELM triggering in ITER with edge stability calculations. Also, projection for reactors remains an outstanding issue.

Flowing liquid metal PFCs

Liquid metal PFCs are being considered as an alternative to solid PFCs for reactors, due to the extreme conditions of simultaneous plasma-material interaction from particle and heat flux, and neutron bombardment. The liquid metal PFCs separate the PMI, which occurs in the near surface layer of the liquid, from the neutron flux, which must be handled by the substrate material. There are a number of fusion devices that have done research with liquid metal PFCs, including T-3, CDX-U, T-11M, FTU, NSTX, LTX, HT7 and EAST. Most of the R&D has been done with liquid Li, which improves energy confinement; a few studies with liquid Sn have also been initiated. Here we give examples of two recent studies using flowing liquid lithium limiters: in HT-7 and EAST.

Two flowing Li limiters were tested in the HT-7 device (Fig. 4)²⁹: a gravitationally driven flowing liquid

lithium (FLiLi) limiter (left panel), and a plate with limit metal infused trenches (LIMIT) that **TEMHD** driven uses flow³⁰. Both limiters were compatible with robust ohmic plasma operation; a reduction marked emission D_a light was observed, indicating reduced recycling flux.

A new version of the FLiLi device was built for EAST. This first generation FLiLi limiter

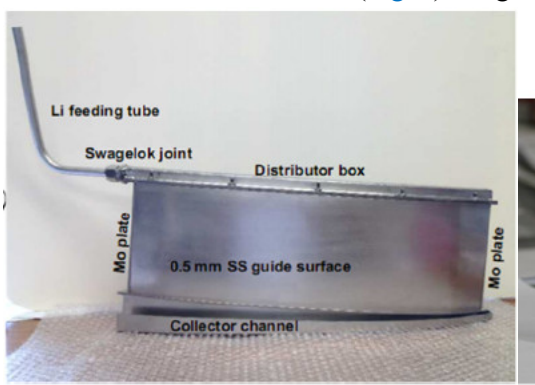


Fig. 4: Two flowing liquid metal limiters tested in the HT-7 device: a gravity driven flowing liquid lithium (FLiLi) limiter (left panel), and a plate with limit metal infused trenches (LIMIT) that uses TEMHD driven flow.

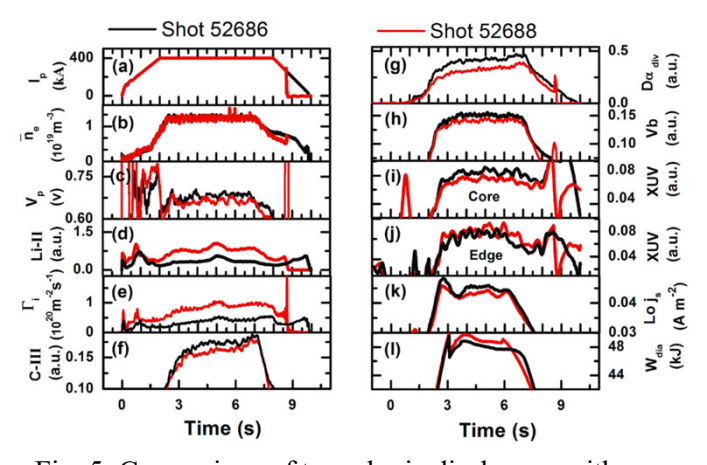


Fig. 5: Comparison of two ohmic discharges with a flowing liquid lithium limiter inserted at the EAST midplane, with (red) and without (black) Li flow. [6]

consisted of a plate made of copper (Cu), due to its high thermal conductivity, covered with a 0.1mm thick layer of stainless steel to prevent Li-Cu reactions⁶. A stainless steel distributor with small holes was attached to the top of the plate, while a stainless steel collector was affixed to the bottom. A j x B magnetic pump drove the liquid lithium from the collector to the distributor, while flow down the limiter surface was gravity-driven. Plate-embedded heaters maintained a minimum temperature above the Li melting point of 180.5 °C, and inlet and outlet tubes were attached to the back of the limiter for He gas cooling. Li was loaded into the FLiLi limiter via a transfer box, and the limiter assembly was inserted into EAST on the Material And Plasma Evaluation System (MAPES) apparatus. To summarize the first

Trench

results⁶: the FLiLi limiter was compatible with ohmic plasmas (Fig. 5), and also RF-heated H-modes, even when placed within 1 cm of the separatrix, with modest improvements in plasma performance. During times of strong PMI, intense green light emission from the plasma indicative of singly charged Li ions was observed, qualitatively similar to plasma emission during Li powder injection. Inspection of the limiter after exposure revealed marked damage on the right side (ion drift side), due to PMI. In particular localized regions where the stainless steel coating had been removed and Li interacted with the underlying copper were evident. In addition the distributor developed a large crack that connected the small hole, preventing uniform flow along the surface. Two upgraded versions of the FLiLi device were tested during the previous project period, as described in the next section.

The LiMIT concept³⁰, developed at the UI-UC, uses TEMHD to flow liquid lithium^{31, 32}. This uses the same principle as thermocouples, where two dissimilar metals produce a thermo-electric voltage via the Seebeck Effect. Li has one of the largest Seebeck coefficients^{33, 34} with respect to stainless steel, W and Mo. LiMIT uses a series of solid metal trenches filled with liquid lithium in a tile design (Fig. 6). As a heat flux source is incident on the surface of the trenches, for example a divertor heat stripe or at the first wall the SOL plasma, the lithium and trenches heat up and produce a voltage. The bottom of the trenches is attached to a bulk heat sink that has cooling lines running through it which will cool the bottom of the trenches. A

different voltage will be generated. Thus, with a temperature gradient in a conducting liquid, a current is formed and returns in the solid trenches. The trenches are situated perpendicular to the toroidal magnetic field then a $J \times B$ force is established and flows the liquid metal. This is the base of the TEMHD pump that can flow the lithium with no moving parts³⁵.

The LiMIT concept has been experimentally verified in laboratory experiments. LiMIT was tested in UI-UC's high heat flux device, SLiDE³⁵, and demonstrated the flowing metal using an electron beam as the heat flux source. It was also tested in HT-7 demonstrating its ability to operate within a larger fusion device³⁶. Its ability to operate in high heat fluxes was also shown at MAGNUM-PSI³⁷. In DeVEX as part of the TELS project LiMIT was shown to be able to operate

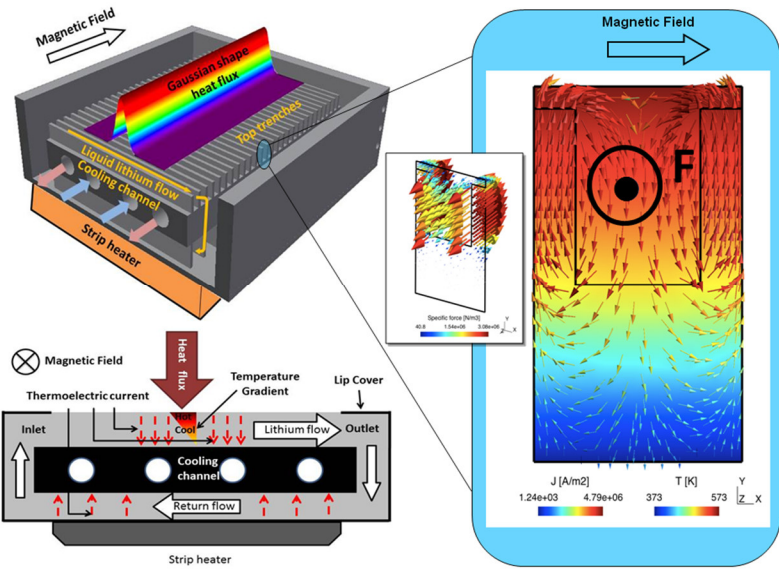


Figure 6: 3-D and sectional schematics of Liquid Metal Infused Trenches (LiMIT) explaining how the temperature gradient produces a thermo-current which in-turn creates flow due to a $J \times B$ force. Upper right shows current density and specific force calculations for typical operating conditions. [30-32]

at different angles, not just horizontally³⁸ and high energy pulsed plasmas showed that with the right trench design the high surface tension of lithium will ensure that there is no material ejection from the exposed flowing surface³⁹.

1.2 Results

Wall conditioning and performance enhancement, ELM suppression, and power exhaust enhancement

EAST: Lithium powder was injected via a conventional powder dropper based on a design originally used in NSTX¹². Since the first ELM suppression results in EAST that used carbon PFCs¹³, the upper divertor in EAST had been replaced with an ITER-style tungsten mono-block. Results from AUG with metallic PFCs using Li pellet injection had not shown neither performance enhancement nor ELM modification⁴⁰; this raised the possibility that Li stability and confinement benefits may occur only in devices with low-Z PFCs. New experiments were therefore conducted with Injection of solid Li microspheres using the new W upper divertor in EAST. These new experiments were successful: ELMs were eliminated in discharges with Li powder injection using the upper tungsten divertor⁴¹; Li powder injection and conditioning also contributed to the achievement of record 100 s pulse lengths in EAST⁴². The likely cause of the edge stability improvement that resulted in ELM stabilization is pedestal-localized turbulence and/or recycling reduction that resulted in a density and pressure profile change, mirroring results with Li evaporation in NSTX⁴³ and Li injection in DIII-D⁸.

Fig. 7 compares four discharges in EAST: three in a sequence with constant Li injection rate, followed

a few discharges later by an ELMy H-mode reference with no Li powder⁴¹. In addition to progressively easier ELM suppression in the discharge sequence, the baseline D_{α} was continuously reduced, indicating a progressive conditioning effect, as also observed in NSTX with pre-discharge Li evaporation⁴³. Note that the stored energy was decreased by up to 10% in the final discharge; we hypothesize that because recycling continues to be reduced even at a constant Li injection rate, a reduced Li powder injection rate could have been used with increasing shot number, to maintain ELM suppression with the minimal effect on density and stored energy.

Analysis of the recycling reduction aimed to quantify the change in divertor recycling

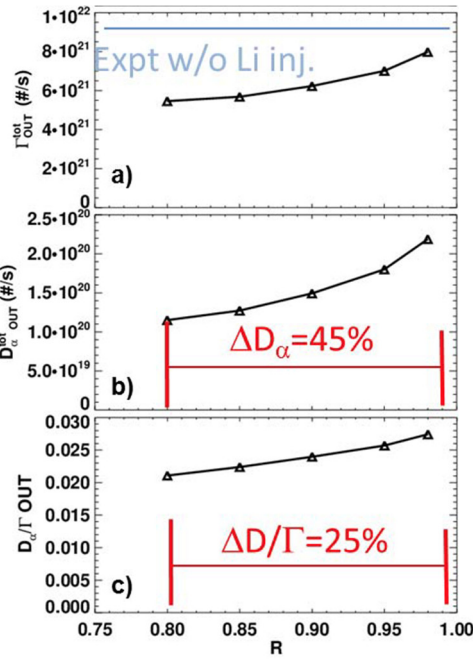


Fig. 8: results of SOLPS analysis of discharges with ELM suppression by Li powder injection. A net reduction of the recycling coefficient by ~ 25% is the best match to the data.

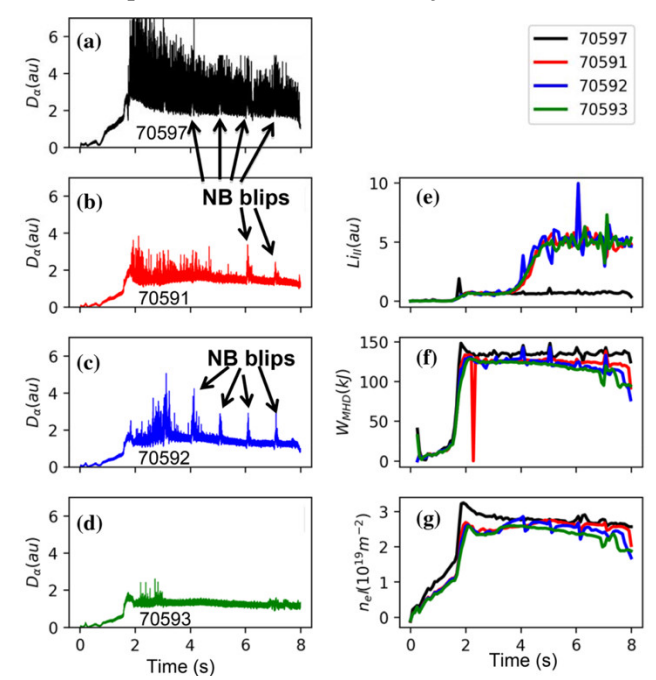


Fig. 7: Upper divertor D_{α} emission from (a) reference #70597, (b) first discharge with dropper #70591, (c) second discharge with dropper #70592, (d) third discharge with dropper #70593. Also shown in panel (e) is the Li-II line emission (f) the plasma stored energy, W_{MHD} , and (g) the line density from the POINT diagnostic. [41]

coefficient with Li powder injection in EAST⁴⁴. A variation of the divertor recycling coefficient was used to generate plasma states in SOLPS, with two values of the upstream separatrix density since the separatrix location has substantial uncertainty. The analysis showed that the experimental value of the outer dvertor baseline particle flux could be reproduced at near-unity recycling before Li powder injection, and that powder injection dropped the recycling coefficient by about 25% (Fig. 8)⁴⁴. The uncertainties in this analysis are unfortunately relatively large, due to lack of heat flux data from IR thermography; that will be remedied in the next project period with the implementation of a new long wavelength IR camera.

AUG and KSTAR: Whereas the use of Li injection has limited (but growing) interest in the worldwide community, due to safety and tritium retention issues, B is a more common choice for wall conditioning. A new IPD was designed by staff at the Princeton Plasma Physics Laboratory (PPPL) to inject a wider range of impurity species than the original dropper, include boron compounds³. This IPD is now deployed on the ASDEX-Upgrade, DIII-D, EAST and KSTAR devices, and one will soon be installed on LHD. The new design is based on an original design that dropped spherical, non-sticky impurities through an aperture on a vibrating piezoelectric disk driven at resonant frequencies; the injected impurities accelerated via gravity into a drop tube and into the boundary plasma¹². The IPD uses piezoelectric crystals for a horizontal drive off the edge of a surface into a drop tube, and is compatible with a wide range of impurity species and particle sizes, including boron-based compounds³. The IPD consists of four reservoirs that can each hold a separate material. Powders fall from the reservoirs onto troughs that, when vibrated by piezoelectric actuators, drop the powder into a common drop tube and into the plasma (Fig. 9). The orientation and mechanical resonant frequency of each of the four sub-systems is set to minimize incidental dropping of powders in separate reservoirs. The dropped powders pass through an optical flow meter in order to monitor the flow rate, and a photodiode mounted at the top points down the length of the drop tube to watch for light emission from the plasma when powders reach the plasma periphery. An example of the calibrated flow rate for two difference materials is shown in Fig. 9c. The powders fall a total distance of several meters, depending on the specific implementation at each site.

Experiments carried out in the ASDEX-Upgrade (AUG) and KSTAR tokamaks, explored the utility of real-time boron coating generation, via injection of B and B enriched powders during tokamak operation.

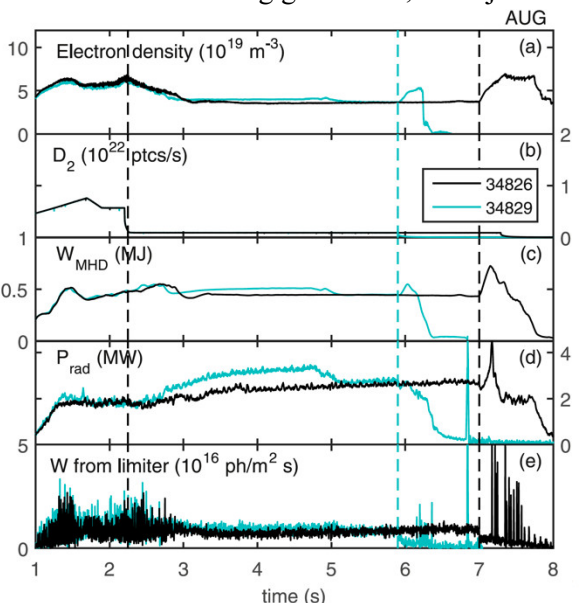
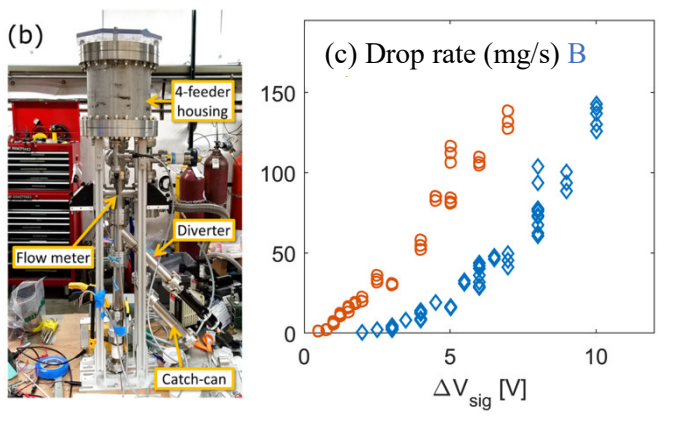


Fig. 10: comparison of two discharges with ELM suppression by magnetic

These results complement the DIII-D results with B conditioning described in the previous section. Wall conditioning improvement similar to boronization was observed in AUG (tungsten PFCs) following injection of pure B and boron nitride (BN) powder into H-mode plasmas designed to condition the walls^{22, 45}. These discharges were taken 18 days and 104 discharges after a conventional gaseous diborane boronization, at which



perturbations, following a sequence of B conditioning discharges. No B. Was a perturbation of one dropper feeder, (b) assembled apparatus in in these discharges. [22] lab with four feeders, and (c) calibrated drop rate for B and Li [3].

point the conventional boronization conditioning effect had worn off. Fig. 10 compares the time evolution of two such discharges in AUG: both had low gas puffing for low density/collisionality, and magnetic perturbations for ELM suppression. While there were modest differences between these identically programmed discharges, there was no evidence of a degradation of wall conditions between them. Thus it can be concluded that the conditioning effect from one or two high B injection rate conditioning discharges lasts for at least 4 subsequent discharges, at least 30 shot seconds, and a cumulative 200 MJ of input energy. Finding the conditioning lifetime requires additional experiments,

the subject of future experiments. Other measured improvements due to the B conditioning at high injection rates included reduction of O and W influx from limiters. For completeness we note that boron injection into ELMy H-Mode KSTAR discharges was tried and showed reduced recycling, similar to DIII-D and AUG, but also mitigation of ELMs. This ELM mitigation effect in KSTAR was even more pronounced with BN injection, as discussed in the next paragraph.

Conceptually BN injection is of interest because of the potential effects of N to enhance radiated power, combined with the positive effects of B for wall conditioning. BN injection into AUG increased both the radiated power (by > 100%) and energy confinement (by 10-20%) (Fig. 11), similar to N₂ gas injection. Moreover the generation of ammonia was reduced by more than 90% with solid BN injection, as compared to gaseous N₂ injection^{45, 46}. In comparison, the first BN injection in KSTAR H-mode discharges resulted in substantial changes in ELM stability: 5 sec long ELM-quiescent phases were observed (graphite PFCs), along with clear changes in edge turbulence relative to the ELMy H-mode with ~ 100 Hz ELMs¹⁰. Fig. 12 shows that the effect in KSTAR depends on the injection rate: short bursts at high injection rate are more effective at ELM suppression than long bursts at low rates. Note that due to time delays in the drop tube, the injection starts about one second after the orange time markers in the figure, and lasts for at least one sec longer than the programmed duration, obviating causality assessment via time correlation.

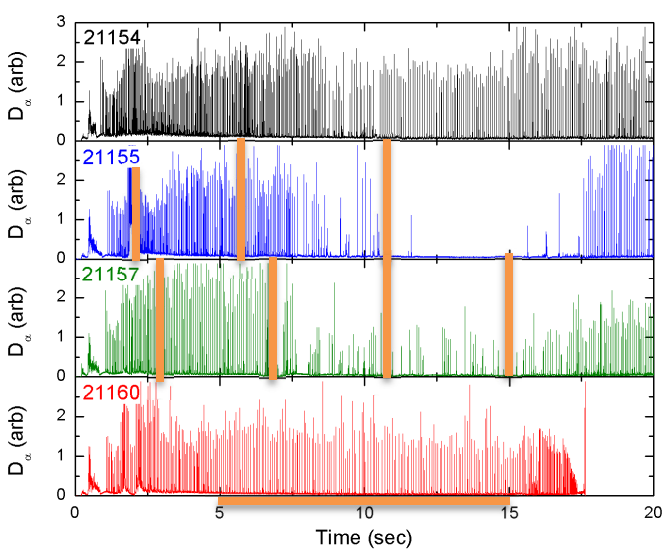


Fig. 12: comparison of BN injection in KSTAR with a reference ELMy H-mode. The injection rates and times are indicated in the captions; note there is a substantial delay trigger > 1 sec. Courtesy of E.P. Gilson, present at the 2019 KSTAR conference, Feb. 20-22, 2019.

size threshold necessary to create a sufficiently large pressure perturbation to destabilize 3D ballooning modes. Experimentally this requires the ability to inject multiple pellet sized and velocities to identify a ELM triggering threshold. The lithium granule injector on EAST was equipped with four reservoirs for independent selection of granule sizes: 300 μm , 500 μm , 700 μm , and 900 μm , with nominal variability of 100 μm each. The maximum granule injection frequency through the LGI decreases rapidly with increasing granule size. Dedicated

ELM mitigation via ELM pacing with impurity pellets in EAST

34802 34799 34801

As stated in the background section, the ability to trigger ELMs with pellet injection depends on predicting and identifying a pellet

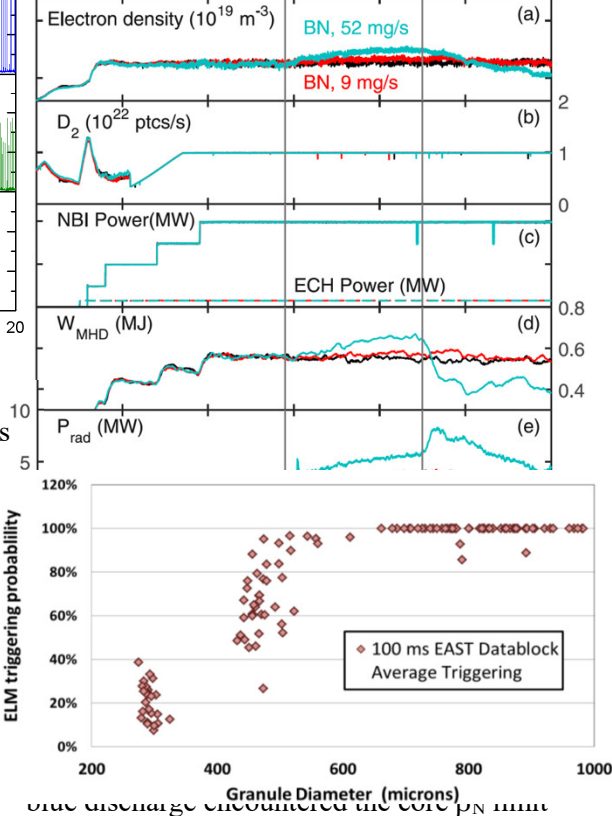


Fig. 213 a ELM soring of the basility we are ided grantile sized back or in planet in overed granules at ~ 100 m/s in EAST, indicating a size threshold.

experiments have identified a size threshold of \geq 500 µm Li granules for ELM triggering on EAST⁴⁷ (Fig. 13), in agreement with complementary experiments on DIII-D²¹. However the natural ELM frequency of the available discharges was \sim 200-250 Hz, i.e. well above the maximum injection capability of LGI granules at 700 µm and 900 µm. Thus it was not possible to assess whether the peak heat flux was affected with ELM triggering. It was however observed that use of 300 µm at 800 Hz injection frequency increased the overall ELM frequency to 600 Hz, despite the fact that each granule did not trigger an ELM⁴⁸. Rather the edge stability was changed via granule injection to a smaller, more rapid ELM regime, with reduced peak heat flux. The extrapolability of such a technique, ELM frequency enhancement without 1:1 pellet-ELM pacing, to future devices merits further investigation.

Good progress was made on granule ablation and penetration physics. The ablation rate of the injected granule(G), in accordance with the NGS model^{16, 49, 50} is proportional to the granule shielding factor η and governed by the equation:

$$G = \frac{8\pi}{25} q_s \eta \xi_g$$
 where q_s is the heat flux to the granule as defined by:

$$q_s = \frac{1}{2} n_e T_e \left(\frac{8T_e}{\pi m_e}\right)^{1/2}$$
 with n_e, T_e and m_e as the electron density, temperature and mass respectively. The granule physical parameters are subsumed within the variable ξ_g which contains the granule radius r_g, the granule density n_g,

the sublimation energy of the granule ΔH and the granule surface temperature T_s and is denoted by

$$\xi_g = \frac{r_g^2}{n_g} \left[\Delta H + \frac{10}{3} T_S \right]^{-1}$$
 In this model, the only unknown parameter *a priori* is the granule shielding factor η , nominally a measure of the effectiveness of the granule at shielding the incoming flux. This was used as an adjustable

parameter. Since adjusting the granule shielding factor varies the temporal duration of an ablation event, the NGS model was benchmarked by matching the calculated and observed ablation times. Granule injection into EAST discharges was simulated with averaged Thomson scattering data for the edge profiles.

The granule shielding factor for lithium granule injections into DIII-D was found²⁶ to be approximately 0.3 and this value was utilized for the first simulations of granule injection into EAST. With $\eta = 0.3$, the calculated ablation duration of 1.3 ms was very close to the recorded granule ablation time of 1.2 ms. However this same granule shielding factor overestimated the ablation time for small granules, thus over estimating the penetration depth, indicating missing physics in this model.

Built upon previous work in mass injection technology development, fast imaging and coupling of experimental data with physics-driven models⁵¹⁻⁵⁵, LANL and collaborators have led and contributed to the impurity injection studies in three directions during the previous funding cycle: a.) Experimental characterization of pellet-plasma interactions by demonstrating a new dual-filter technique⁵⁶; b.) Supplying pellet ablation models to the BOUT++ code in order to simulate and predict impurity pellet penetration, and c.) Introduction of hollow pellet injection concept for magnetic fusion applications⁵⁷. The three activities are distinct and closely coupled to each other. The dual-filter imaging technique is to collect high-resolution images of pellet ablation for modeling and understanding of the pellet transport and ablation (e.g. Fig. 14). The model development through collaboration is for experimental data explanation and further improvements of injection technology. The efforts in experiment and modeling culminated in the new hollow pellet injection concept that is attractive to steady-state long-pulse plasma operations including in-

situ wall conditioning, ELM control, power and particle exhaust control, impurity transport, etc. as explained in other sections of the proposal.

Better understanding of injected-mass-plasma interactions requires spatially and temporally resolving diagnostics that can characterize the in-situ dynamics of the mass interactions with plasmas. Fast imaging can be used to characterize the ionization dynamics such as the propagation of the ionization front, which





Fig. 14: (Top) An image of a lithium granule ablation in the EAST experiment; (Bottom) similar image of a lithium granule image when using a dual-wavelength filter to demonstrate resolution of the granule from the ablation plasma background [57].

moves at the thermal sound or higher speed, and mixing of the neutral atoms with the ambient plasma. Multi-wavelength spectral imaging is promising since different parts of the plasma give away different spectral signatures. We demonstrated a dual-spectral imaging technique based on a monochromatic camera (Vision Research) sensor and filters with two narrow bandwidth passing optical wavelengths. The method is shown to improve image contrast significantly as shown in Fig. 14 for similar cases with and without the filter. In addition to its simplicity, the techniques also compare favorably with alternatives such as color cameras and methods using a filter wheel. Further improvements through relative filter area ratios and plenoptic imaging were previously described⁵⁶. We also plan to extend the technique to other wavelengths.

Flowing liquid metal PFCs in EAST

Due to its strong chemical reactivity with vacuum impurity gases, maintaining a clean Li plasma-facing surface for hydrogen pumping requires continuous flow for long pulse discharges, a key purpose of the flowing liquid Li (FLiLi) limiter program in EAST^{6, 58, 59}. Three generations of limiters have now been exposed to EAST H-mode plasmas. Table 1 compares their design characteristics, and the types of plasmas exposed to them.

Table 1: Comparison of three generations of the FLiLi limiter

Generation	Heat Sink	SS thickness (mm)	JxB pumps	Max. P _{aux} (MW)	Max. q _{exh} (MW/m ²)	Max. W _{MHD} (kJ)
1	Cu + SS	0.1	1	1.9	3.5	120
2	Cu + SS	0.5	2	4.5	4	170
3	Mo (TZM)	NA	2	8.3	TBD	280

A 2^{nd} generation flowing liquid Li limiter was designed with several upgrades⁶⁰ to prevent the damage observed in the 1^{st} generation system. First a thicker stainless steel protective layer (0.5mm vs. 0.1 mm) was used to prevent PMI from exposing the Cu heat sink to the liquid Li. Next an additional j x B magnetic pump was added for a more uniform supply of Li to the distributor on the top of the limiter. In addition, surface texturing was implemented in the 2^{nd} generation, which improved the wetting uniformity of the liquid Li flowing on the front face. Also, an improved method for manufacturing the top Li distributor from

two pieces was developed; this new design avoided the crack that developed during deployment of the 1st generation distributor.

The $2^{\rm nd}$ generation limiter was inserted into plasma discharges on two separate dates⁶¹, demonstrating an ability to restart Li flow after it has been stopped for more than a week. Camera images after the first exposure showed a relatively pristine limiter surface, but photographs after the second exposure showed streaks on the plasma-facing surface, indicating the formation of surface-contaminating compounds that may have hindered free flow in the second exposure. The limiter plate condition after plasma exposure for the $2^{\rm nd}$ generation showed no visible damage, whereas the $1^{\rm st}$ generation limiter showed visible damage on the right hand side of the limiter face^{59, 60}. In addition the fractional surface area that was un-wetted by the Li was < 20% in Gen 1, vs. $\sim 70\%$ in Gen. 2.

The upper divertor D_{α} emission and ELM size were continuously reduced in otherwise constant discharge conditions into which the 2nd generation limiter was inserted⁶¹: plasma current $I_p = 0.45$ MA, toroidal field $B_t = -2.5$ T, $P_{aux}=2.9$ MW, in an upper single-null configuration with ion grad-B drift toward the lower divertor. These results showing progressive conditioning and ELM mitigation are qualitatively

similar to Li powder injection on EAST⁴¹, as well as with pre-discharge Li evaporation in NSTX⁴³. Finally, short-lived *true* ELM-free phases (and also ohmic H-modes) were observed for the first time in EAST with increasing τ_E and transient $H_{H98y2} \leq 2$ when the 2nd generation limiter was inserted. We refer to these as *true* ELM-free H-modes because of the density accumulation observed, which is not seen in the ELM suppressed cases observed with e.g. real-time Li powder injection.

The performance of the limiter and plasma characteristics is shown as a function of increasing auxiliary power⁶¹ in Fig. 15. It can be seen that the limiter temperature rise from near-surface thermocouples, the plasma Li-II emission, and the Fe-XV emission all increase with increasing P_{aux}. The increasing Fe emission, likely from PMI with dry spots on the limiter surface, and/or with the

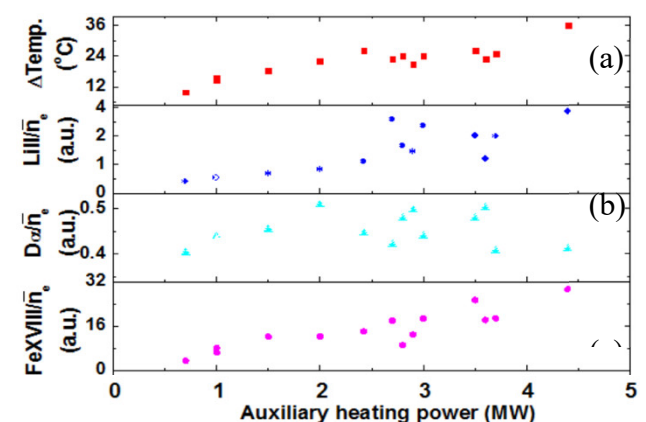


Fig. 15: Performance of 2^{nd} generation limiter and plasma emission vs. auxiliary heating power P_{aux} : (a) limiter temperature rise, (b) Li-II emission, (c) D_{α} emission, and (d) Fe-XVIII emission, normalized by line-average density. [61]

distributor or collector, motivated use of a substrate more resistant to sputtering, e.g. W or Mo. Using a 1-D infinite slab thermal conduction model, we computed from the thermocouple temperature rise that a peak heat flux $\sim 4~MW/m^2$ was exhausted by the 2^{nd} generation FLiLi in the discharge with $P_{aux} \sim 4.5~MW^{61}$.

Due to the continuing success of the FLiLi limiter program, a 3^{rd} generation limiter constructed entirely of TZM, an alloy with > 99% Mo, was fabricated by conventional manufacturing techniques⁶². Mo was chosen due to its higher sputtering resistance, as compared to stainless steel, and its good compatibility with conventional manufacturing, as compared to tungsten. The front face of the limiter was polished for a mirror-like finish to facilitate flow. The 3^{rd} generation FLiLi was inserted into the edge of EAST H-mode plasmas in an upper single-null configuration with ion grad-B drift toward the upper divertor. Fig. 16 compares⁶² a reference discharge (black) with one in which the FLiLi limiter was inserted to within 3 cm of the separatrix (red) with $I_p = 0.55$ MA, $B_t = 2.5$ T, $P_{aux} = 7.9$ -8.3 MW, EM pump current = 100 A. The neutral Li line emission is higher with the limiter inserted, as expected, while the D_{α} emission from the upper divertor is substantially lower. The stored energy is slightly higher with the limiter inserted, though this is partly due to modestly higher heating power. The line-average density is comparable. Overall the limiter performed well for this set of discharges. Upon removal, however, damage to the electron drift side of the limiter plate was evident, as was damage to the right hand side of the collector. The reasons for the

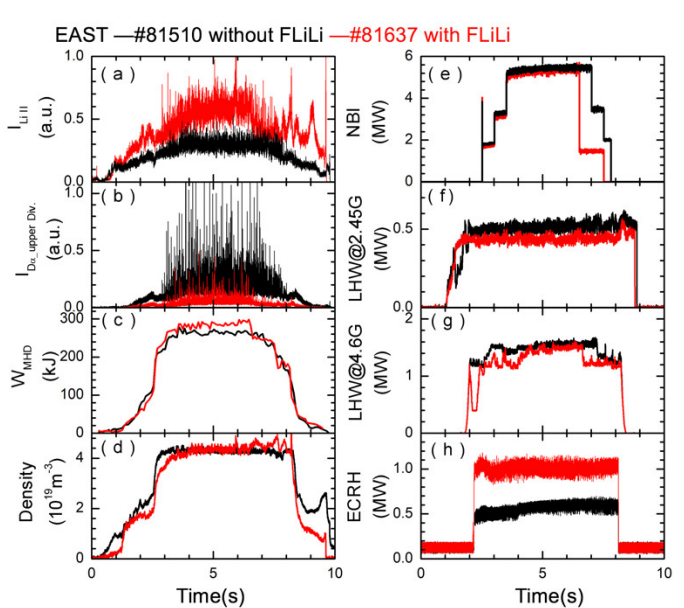


Fig. 16: Comparison of plasma with (red - #81637) and without (black-#81510) the 3^{rd} generation FLiLi limiter inserted: (a) Li-II emission, (b) Upper divertor D_{α} emission, and (c) Plasma stored energy, (d) line-average density, (e) neutral beam injected power, (f) low frequency lower hybrid power, (g) high frequency lower hybrid power, and (h) electron cyclotron resonant heating power. The auxiliary heating power with FLiLi was 6% higher, partly resulting in higher stored energy. [62]

In addition to the exposure of FLiLi limiters in EAST H-mode plasmas, significant progress was made on manufacturing of LIMIT limiters for EAST. Two plates with LIMIT groves were manufactured, and brazing of He cooling lines is progressing, with the goal of exposing LIMIT in EAST H-mode plasmas in the summer of 2019. A second set of LIMIT plates, scaled down by $\sim 10\%$ to fit within HIDRA, are being manufactured.

damage are under investigation.

Surface science experiments in EAST First wall conditioning and material injection influence long-pulse operation and plasma performance in tokamaks. More specifically, the physical and chemical interaction of the plasma and neutral gas with the plasma-facing components (PFCs) affects fuel recycling and retention. Net erosion of PFCs also defines a source of impurities and is a crucial factor to understand material migration in a tokamak. With low-Z wall conditioning, erosion and migration of high-Z impurities is exacerbated because wall conditioning materials, such as lithium and boron, are more efficient at

sputtering molybdenum and tungsten than deuterium. Net erosion rates are, however, notoriously difficult to measure in tokamaks, due to limited diagnostic access and the competing processes of gross erosion and prompt re-deposition, as well as deposition from long-range material migration. Deposited depth marker layers have been used in the past to measure campaign-averaged net erosion rates in tokamaks⁶³. While this allows for a distinct and well-defined depth marker, it involves deposition of multiple layers rather than working with bulk materials. For the proposed work we use selected isotopes as depth markers, which we implant at known depth in

bulk materials using an ion accelerator and analyze with a different beam with the same

accelerator. This technique has the advantage of using bulk materials and can be combined with traditional ion beam analysis techniques to characterize the elemental composition of the surface and/or plasma-deposited layers, yielding valuable information on net erosion sources, material migration, and retention properties during long-pulse operations. Figure 17 shows the spectra of three samples with fluorine on or implanted in the material.

The implanted depth marker technique for ex situ analysis has been developed for net erosion measurements in EAST. We have utilized the Material And Plasma Exposure System (MAPES) for outboard mid-plane exposure (flowing liquid Li limiters are also mounted⁶⁴ on MAPES). We have installed modified first wall tiles for exposure to the inboard midplane (Fig. 18). Analysis of these samples is in progress.

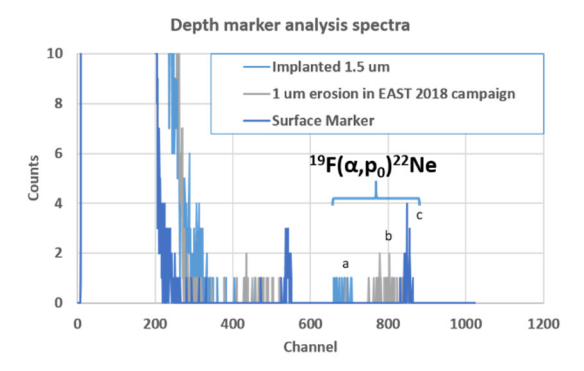


Fig. 17: Nuclear reaction analysis of the implanted depth marker a) before and b) after exposure on the HFS in EAST for the 2018 campaign compared to c) a LiF surface marker. Courtesy of Dr. Kevin



Fig. 18: Pictures of implanted samples mounted in modified first wall tiles on the high field side in EAST (top row) and on MAPES located at the H port (bottom row). Courtesy of Yudong Xie, ASIPP.

Appendix 3: Bibliography and references cited

- 1. J. Winter, 1996 Plasma Phys. Control. Fusion 38 1503
- 2. H. W. Kugel, M. G. Bell, J. W. Ahn, J. P. Allain, R. Bell, J. Boedo, C. Bush, D. Gates, T. Gray, S. Kaye, R. Kaita, B. LeBlanc, R. Maingi, R. Majeski, D. Mansfield, J. Menard, D. Mueller, M. Ono, S. Paul, R. Raman, A. L. Roquemore, P. W. Ross, S. Sabbagh, H. Schneider, C. H. Skinner, V. Soukhanovskii, T. Stevenson, J. Timberlake, W. R. Wampler, and L. Zakharov, 2008 *Phys. Plasmas* 15 056118
- 3. A. Nagy, A. Bortolon, D.M. Mauzey, E. Wolfe, E.P. Gilson, R. Lunsford, R. Maingi, D.K. Mansfield, R. Nazikian, and A. L. Roquemore, 2018 *Rev. Sci. Instrum.* **89** 10K121
- 4. D. K. Mansfield, A. L. Roquemore, T. Carroll, Z. Sun, J. S. Hu, L. Zhang, Y. F. Liang, X. Z. Gong, J. G. Li, H. Y. Guo, G. Z. Zuo, P. Parks, W. Wu, and R. Maingi, 2013 *Nucl. Fusion* **53** 113023
- 5. A. Nagy, A. Bortolon, W. Brown, P. Fisher, R. Lunsford, R. Maingi, D. Mansfield, D. Mauzey, R. Nguyen, and M. Vorenkamp, 2018 *IEEE Trans. Plasma Sci.* **46** 1120
- 6. J. S. Hu, G.Z. Zuo, J. Ren, Q. X. Yang, Z.X. Chen, H. Xu, L.E. Zakharov, R. Maingi, C. Gentile, X. C. Meng, Z. Sun, W. Xu, Y. Chen, D. Fan, N. Yan, Y.M. Duan, Z.D. Yang, H.L. Zhao, Y.T. Song, X.D. Zhang, B.N. Wan, J.G. Li, and E. team, 2016 *Nucl. Fusion* **56** 046011
- 7. G. L. Jackson, J. Winter, T. S. Taylor, K. H. Burrell, J. C. DeBoo, C. M. Greenfield, R. J. Groebner, T. Hodapp, K. Holtrop, E. A. Lazarus, L. L. Lao, S. I. Lippmann, T. H. Osborne, T. W. Petrie, J. Phillips, R. James, D. P. Schissel, E. J. Strait, A. D. Turnbull, W. P. West, and D.-D. Team, 1991 *Phys. Rev. Lett.* 67 3098
- 8. M. G. Bell, H. W. Kugel, R. Kaita, L. E. Zakharov, H. Schneider, B. P. LeBlanc, D. Mansfield, R. E. Bell, R. Maingi, S. Ding, S. M. Kaye, S. F. Paul, S. P. Gerhardt, J. M. Canik, J. C. Hosea, and G. Taylor, 2009 *Plasma Phys. Control. Fusion* **51** 124054
- 9. R. Maingi, S. M. Kaye, C. H. Skinner, D. P. Boyle, J. M. Canik, M. G. Bell, R. E. Bell, T. K. Gray, M. A. Jaworski, R. Kaita, H. W. Kugel, B. P. LeBlanc, D. K. Mansfield, T. H. Osborne, S. A. Sabbagh, and V. A. Soukhanovskii, 2011 *Phys. Rev. Lett.* **107** 145004
- 10. R. Maingi, T.H. Osborne, B. P. LeBlanc, R. E. Bell, J. Manickam, P. B. Snyder, J. E. Menard, D. K. Mansfield, H. W. Kugel, R. Kaita, S. P. Gerhardt, S. A. Sabbagh, F. A. Kelly, and the NSTX research team, 2009 *Phys. Rev. Lett.* **103** 075001
- D. K. Mansfield, H. W. Kugel, R. Maingi, M. G. Bell, R. Bell, R. Kaita, J. Kallman, S. Kaye, B. LeBlanc,
 D. Mueller, S. Paul, R. Raman, L. Roquemore, S. Sabbagh, H. Schneider, C. H. Skinner, V. Soukhanovskii,
 J. Timberlake, J. Wilgen, and L. Zakharov, 2009 J. Nucl. Mater. 390-391 764
- 12. D. K. Mansfield, A.L. Roquemore, H. Schneider, J. Timberlake, H. Kugel, M. G. Bell, and N. R. Team, 2010 Fusion Eng. Des. 85 890
- J. S. Hu, Z. Sun, H. Y. Guo, J. G. Li, B. N. Wan, H. Q. Wang, S. Y. Ding, G. S. Xu, Y. F. Liang, D. K. Mansfield, R. Maingi, X. L. Zou, L. Wang, J. Ren, G. Z. Zuo, L. Zhang, Y. M. Duan, T. H. Shi, L. Q. Hu, and t. East, 2015 *Phys. Rev. Lett.* 114 055001
- 14. T. H. Osborne, G. L. Jackson, Z. Yan, R. Maingi, D. K. Mansfield, B. A. Grierson, C. P. Chrobak, A. G. McLean, S. L. Allen, D. J. Battaglia, A. R. Briesemeister, M. E. Fenstermacher, G. R. McKee, and P. B. Snyder, 2015 Nucl. Fusion 55 063018
- 15. A. Bortolon, 2018 Bull. Am. Phys. Soc. 63 http://meetings.aps.org/Meeting/DPP18/Session/UP11.41

- 16. P. Parks, J.S. Leffler, and R. K. Fisher, 1988 Nucl. Fusion 28 477
- 17. T. Eich, A. W. Leonard, R. A. Pitts, W. Fundamenski, R. J. Goldston, T. K. Gray, A. Herrmann, A. Kirk, A. Kallenbach, O. Kardaun, A. S. Kukushkin, B. LaBombard, R. Maingi, M. A. Makowski, A. Scarabosio, B. Sieglin, J. Terry, and A. Thornton, 2013 *Nucl. Fusion* **53** 093031
- 18. T. Eich, B. Sieglin, A. Scarabosio, W. Fundamenski, R. Goldston, and A. Herrmann, 2011 *Phys. Rev. Lett.* **107** 215001
- 19. R. J. Goldston, 2012 Nucl. Fusion 52 013009
- M. N. A. Beurskens, J. Schweinzer, C. Angioni, A. Burckhart, C. D. Challis, I. Chapman, R. Fischer, J. Flanagan, L. Frassinetti, C. Giroud, J. Hobirk, E. Joffrin, A. Kallenbach, M. Kempenaars, M. Leyland, P. Lomas, G. Maddison, M. Maslov, R. McDermott, R. Neu, I. Nunes, T. Osborne, F. Ryter, S. Saarelma, P. A. Schneider, P. Snyder, G. Tardini, E. Viezzer, and E. Wolfrum, 2013 *Plasma Phys. Control. Fusion* 55 124043
- A. Bortolon, R. Maingi, D.K. Mansfield, A. Nagy, A.L. Roquemore, L.R. Baylor, N. Commaux, G.L. Jackson, E. Gilson, R. Lunsford, and P. B. Parks, 2016 Nucl. Fusion 56 056008
- A. Bortolon, V. Rohde, R. Dux, R. Maingi, E. Wolfrum, A. Nagy, A. Herrmann, R. Lunsford, R. McDermott, A. Kallenbach, R. Neu, D. Mansfield, R. Nazikian, and A.-U. team, 2019 *Nucl. Mater. Energy* 19 384
- A. Loarte, G. Huijsmans, A. Futatani, S. Futatani, L.R. Baylor, T.E. Evans, D. M. Orlov, O. Schmitz, M. Becoulet, P. Cahyna, Y. Gribov, A. Kavin, A. Sashala Naik, D.J. Campbell, T. Casper, E. Daly, H. Frerichs, A. Kischner, R. Laengner, S. Lisgo, R.A. Pitts, G. Saibene, and A. Wingen, 2014 Nucl. Fusion 54 033007
- 24. G. Huysmans, S. Pamela, E. van der Plas, and P. Ramet, 2009 Plasma Phys. Control. Fusion 51 124012
- 25. S. Futatani, G. Huijsmans, A. Loarte, L.R. Baylor, N. Commaux, T.C. Jernigan, M.E. Fenstermacher, C. Lasnier, T.H. Osborne, and B. Pegourié, 2014 *Nucl. Fusion* **54** 073008
- R. Lunsford, A. Bortolon, A.L. Roquemore, D.K. Mansfield, A. Nagy, R.Maingi, P.B. Parks, G. Jackson, E. Gilson, and C. P. Chrobak. 2016 Fusion Eng. Design 112 621
- 27. P. B. Parks, 2001 Phys. Plasmas 7 1968
- R. Lunsford, A. Bortolon, R. Maingi, D.K. Mansfield, A. Nagy, G.L. Jackson, and T. Osborne, 2019 Nucl. Mater. Energy 19 34
- J. Ren, J. S. Hu, G. Z. Zuo, Z. Sun, J. G. Li, D. N. Ruzic, and L. E. Zakharov, 2014 *Physica Scripta* T159 014033
- 30. D. N. Ruzic, W. Xu, D. Andruczyk, and M. A. Jaworski, 2011 Nucl. Fusion 51 102002
- 31. J. A. Schercliff, 1979 J. Fluid. Mech. 91 231
- 32. M. A. Jaworski, T. K. Gray, M. Antonelli, J. J. Kim, C. Y. Lau, M. B. Lee, M. J. Neumann, W. Xu, and D. N. Ruzic, 2010 *Phys. Rev. Lett.* **104** 094503
- 33. V. Surla, M. Tung, W. Xu, D. Andruczyk, M. Neumann, D. N. Ruzic, and D. Mansfield, 2011 *J. Nucl. Mater.* 415 18
- 34. P. Fiflis, L. Kirsch, D. Andruczyk, D. Curreli, and D. N. Ruzic, 2013 J. Nucl. Mater. 438 224

- 35. W. Xu, D. Curreli, D. Andruczyk, T. Mui, R. Switts, and D. N. Ruzic, 2013 J. Nucl. Mater. 438 S422
- J. Ren, G. Z. Zuo, J. S. Hu, Z. Sun, J. G. Li, L. E. Zakharov, D. N. Ruzic, and W. Y. Xu, 2016 Fusion Eng. Design 102 36
- 37. P. Fiflis, T. W. Morgan, S. Brons, G. G. Van Eden, M. A. Van Den Berg, W. Xu, D. Curreli, and D. N. Ruzic, 2015 *Nucl. Fusion* 55
- 38. W. Xu, P. Fiflis, M. Szott, K. Kalathiparambil, S. Jung, M. Christenson, I. Haehnlein, A. Kapat, D. Andruczyk, D. Curreli, and D. N. Ruzic, 2015 *J. Nucl. Mater.* **463** 1181
- 39. P. Fiflis, M. Christenson, M. Szott, K. Kalathiparambil, and D. N. Ruzic, 2016 Nucl. Fusion 56
- 40. P. T. Lang, R. Maingi, D. K. Mansfield, R. M. McDermott, R. Neu, E. Wolfrum, R. Arredondo Parra, M. Bernert, G. Birkenmeier, A. Diallo, M. Dunne, E. Fable, R. Fischer, B. Geiger, A. Hakola, V. Nikolaeva, A. Kappatou, F. Laggner, M. Oberkofler, B. Ploeckl, S. Potzel, T. Pütterich, B. Sieglin, and T. Szepesi, 2017 Nucl. Fusion 57 016030
- 41. R. Maingi, J. S. Hu, Z. Sun, K. Tritz, G. Z. Zuo, W. Xu, M. Huang, X. C. Meng, J. M. Canik, A. Diallo, R. Lunsford, D. K. Mansfield, T. H. Osborne, X. Z. Gong, Y. F. Wang, and Y. Y. Li, 2018 *Nucl. Fusion* **58** 024003
- 42. Z. Sun, R. Maingi, J.S. Hu, W. Xu, G.Z. Zuo, Y.W. Yu, C.R. Wu, M. Huang, X.C. Meng, L. Zhang, L. Wang, S.T. Mao, F. Ding, D.K. Mansfield, J. Canik, R. Lunsford, A. Bortolon, X.Z. Gong, and E. Team, 2019 Nucl. Mater. Energy 19 124
- 43. R. Maingi, D. P. Boyle, J. M. Canik, S. M. Kaye, C. H. Skinner, J. P. Allain, M. G. Bell, R. E. Bell, S. P. Gerhardt, T. K. Gray, M. A. Jaworski, R. Kaita, H. W. Kugel, B. P. LeBlanc, J. Manickam, D. K. Mansfield, J. E. Menard, T. H. Osborne, R. Raman, A. L. Roquemore, S. A. Sabbagh, P. B. Snyder, and V. A. Soukhanovskii, 2012 *Nucl. Fusion* **52** 083001
- 44. J. M. Canik, Z. Sun, J.S. Hu, G.Z. Zuo, W. Xu, M. Huang, R. Maingi, R. Lunsford, A. Diallo, D. Mansfield, T. Osborne, K. Tritz, and E. Team, 2018 *IEEE Trans. Plasma Sci.* **46** 1081
- 45. R. Lunsford, V. Rohde, A. Bortolon, R. Dux, A. Herrmann, A. Kallenbach, R. M. McDermott, R. Maingi, D. K. Mansfield, A. Nagy, R. Neu, E. Wolfrum, and A.-U. team, 2018 *Proc. 27th Internatonal Conf. on Fusion Energy, Ahmedabad, India, 18-22 Oct. 2018* Paper FIP/2_3; Nucl. Fusion (2019) in preparation
- 46. A. Drenik, 2019 invited talk to be presented at the 2019 Euro. Conf. on Plasma Phys. and Conrol. Fusion, Milan, Italy, 8-12 July 2019
- 47. R. Lunsford, Z. Sun, R. Maingi, J. S. Hu, D. Mansfield, W. Xu, G. Z. Zuo, A. Diallo, T. Osborne, K. Tritz, J. Canik, M. Huang, X. C. Meng, X. Z. Gong, B. N. Wan, and J. G. Li, 2018 *Nucl. Fusion* **58** 036007
- 48. R. Lunsford, J. S. Hu, Z. Sun, R. Maingi, D. K. Mansfield, W. Xu, G. Z. Zuo, M. Huang, A. Diallo, T. Osborne, K. Tritz, J. Canik, X. C. Meng, Q. Zang, X. Z. Gong, B. N. Wan, and J. G. Li, 2018 *Nucl. Fusion* 58 126021
- 49. G. Kocsis, J S Bakos, R Burhenn, B Kardon, S K'alvin, L Ledl, G Mank, G Petravich, A Pospieszczyk, and S. Zoletnik, 1999 *Plasma Phys. Control. Fusion* **41** 881
- 50. P. B. Parks, G.A. Gerdin, L.L. Vahala, and A. G. Elcashlan, 1994 Nucl. Fusion 34 417
- 51. Z. Wang, S. K. Combs, L. R. Baylor, C. R. Foust, M. S. Lyttle, S. J. Meitner, and D. A. Rasmussen, 2014 The Review of scientific instruments 85 11E805

- Z. Wang, Q. Liu, W. Waganaar, J. Fontanese, D. James, and T. Munsat, 2016 The Review of scientific instruments 87 11D601
- 53. Z. Wang, R. Lunsford, D. K. Mansfield, and J. H. Nichols, 2016 Journal of Plasma Physics 82
- 54. Z. Wang, and G. A. Wurden, 2003 Rev. Sci. Instrum. 74 1887
- 55. P. Chu, T. Wolfe, and Z. Wang, 2018 Rev. Sci. Instrum. 89 10K101
- Z. Sun, J. K. Baldwin, W. Xu, Z. Wang, J. Hu, R. Maingi, C. Romero-Talamas, and D. M. Oschwald, 2018 The Review of scientific instruments 89 10E112
- 57. Z. Wang, M. Hoffbauer, E. Hollmann, Z. Sun, Y. Wang, N. Eidietis, J.S. Hu, R. Maingi, J. Menard, and X. Xu, 2019 *Nucl. Fusion* **59** at press
- 58. G. Z. Zuo, J.S. Hu, R. Maingi, J. Ren, Z. Sun, Q.X. Yang, Z.X. Chen, H. Xu, K. Tritz, L.E. Zakharov, C. Gentile, X.C. Meng, M. Huang, W. Xu, Y. Chen, L. Wang, N. Yan, S.T. Mao, Z.D. Yang, J.G. Li, and E. Team, 2017 *Nucl. Fusion* 57 046017
- 59. J. S. Hu, G.Z. Zuo, R. Maingi, Z. Sun, K. Tritz, W. Xu, Q. X. Yang, D. Andruczyk, M. Huang, X. C. Meng, X.Z. Gong, D. N. Ruzic, M.J. Ni, B.N. Wan, J.G. Li, and E. team, 2019 *Nucl. Mater. Energy* **18** 99
- 60. G. Z. Zuo, J. S. Hu, R. Maingi, Q. X. Yang, Z. Sun, M. Huang, Y. Chen, X. L. Yuan, X. C. Meng, W. Xu, C. Gentile, A. Carpe, A. Diallo, R. Lunsford, D. Mansfield, T. Osborne, K. Tritz, and J. G. Li, 2017 *Rev. Sci. Instrum.* 88 123506
- 61. G. Z. Zuo, J.S. Hu, R. Maingi, Z. Sun, Q. X. Yang, M. Huang, X. C. Meng, W. Xu, X.Z. Gong, K. Tritz, A. Diallo, R. Lunsford, J.G. Li, and E. team, 2019 *Nucl. Fusion* **59** 016009
- 62. R. Maingi, J.S. Hu, G.Z. Zuo, D. Andruczyk, J.M. Canik, A. Diallo, K.F. Gan, E. Gilson, X.Z Gong, T.K. Gray, M. Huang, R. Lunsford, D.K. Mansfield, X. C. Meng, T.H. Osborne, D.N. Ruzic, Z. Sun, K. Tritz, W. Xu, Z. Wang, B.D. Wirth, K. Woller, S.J. Zinkle, and E. Team, 2018 *Proc. 2018 Internatonal Conf. on Fusion Energy, Ahmedabad, India, 22-27 Oct. 2018* Paper FIP 3 5 Ra
- 63. W. R. Wampler, B. LaBombard, B. Lipschultz, G.M. McCracken, D.A. Pappas, and C. S. Pitcher, 1999 *J. Nucl. Mater.* **266** 217
- 64. J. Ren, G. Z. Zuo, J. S. Hu, Z. Sun, Q. X. Yang, J. G. Li, L. E. Zakharov, H. Xie, and Z. X. Chen, 2015 *The Review of scientific instruments* 86 023504

Publications and presentations

Refereed Journal Articles

- 1. G.Z. Zuo, J.S. Hu, R. Maingi, J. Ren, Z. Sun, Q.X. Yang, Z.X. Chen, H. Xu, K. Tritz, L.E. Zakharov, C. Gentile, X.C. Meng, M. Huang, W. Xu, Y. Chen, L. Wang, N. Yan, S.T. Mao, Z.D. Yang, J.G. Li, and EAST Team, "Mitigation of plasma–material interactions via passive Li efflux from the surface of a flowing liquid lithium limiter in EAST", *Nucl. Fusion* 57 (2017) 046017.
- 2. L.A. Kesler, B.N. Sorbom, Z.S. Hartwig, H.S. Barnard, G.M. Wright, and D.G. Whyte, "Initial results of tests of depth markers as a surface diagnostic for fusion devices", *Nucl. Mater. Energy* **12** (2017) 1277.
- 3. G.Z. Zuo, J.S. Hu, R. Maingi, Q. X. Yang, Z. Sun, M. Huang, Y. Chen, X.L. Yuan, X. C. Meng, W. Xu, J.G. Li, C. Gentile, A. Carpe, A. Diallo, R. Lunsford, D.K. Mansfield, K. Tritz and EAST team, "Upgraded flowing liquid lithium limiter for improving Li coverage uniformity and erosion resistance in EAST device", *Rev. Sci. Instrum.* 88 (2017) 123506.
- 4. H. Lan, G. S. Xu, K. Tritz, N. Yan, T. H. Shi, Y. L. Li, T. Wang, L. Wang, J. Chen, Y. M. Duan, Y. Yuan, Y. Sun, S. Gu, Q. Zang, R. Chen, L. Cheng, X. Zheng, S. Chen, H. Liu, Y. Ye, H. Wang, B. N. Wan, "Analysis of electron temperature, impurity transport and MHD activity with multi-energy soft x-ray diagnostic in EAST tokamak," *Plasma Sci. Tech.*, 19, 125101 (2017)
- 5. R. Maingi, J.S. Hu, Z. Sun, G.Z. Zuo, W. Xu, Q. X. Yang, M. Huang, X. C. Meng, A. Diallo, R. Lunsford, D. Mansfield, T. Osborne, K. Tritz and EAST team, "ELM suppression with Li powder injection in EAST discharges using the tungsten upper divertor", *Nucl. Fusion* **58** (2018) 024003.
- R. Lunsford, Z. Sun, R. Maingi, J.S. Hu, D. Mansfield, W. Xu, G.Z. Zuo, T. Osborne, K. Tritz, A. Diallo, M. Huang, X. C. Meng, X. Z. Gong, B.N. Wan, J.G. Li, and the EAST team, "Threshold levels for lithium granule instigated high frequency pacing of edge localized modes on EAST", *Nucl. Fusion* 58 (2018) 036007.
- 7. X. Meng, G. Zuo, W. Xu, Z. Sun, M. Huang, X. Yuan, C. Xu, W. Hu, D. Andruczyk, J. Hu, H. Deng, "The effect of temperature on corrosion behaviour of 304 stainless steel in static liquid lithium", *Fusion Eng. Design* **128** (2018) 75.
- 8. Z. Sun, R. Lunsford, R. Maingi, J.S. Hu, D. Mansfield, A. Diallo, K. Tritz, W. Xu, J. Canik, Z. Wang, D. Andruczyk, Y.M. Wang, G.Z. Zuo, M. Huang, W. Xu, X. C. Meng, and EAST team, "First results of ELM triggering with a multi-chamber lithium granule injector into EAST discharges", *IEEE Trans. On Plasma Sci.* 46 (2018) 1076.
- 9. J. M. Canik, Z. Sun, J.S. Hu, G.Z. Zuo, W. Xu, M. Huang, R. Maingi, R. Lunsford, A. Diallo, D. Mansfield, T. Osborne, K. Tritz, and EAST Team, "Active recycling control through lithium injection in EAST", *IEEE Trans. On Plasma Sci.* 46 (2018) 1081.
- A. Nagy, A. Bortolon, W. Brown, P. Fisher, R. Lunsford, R. Maingi, D. Mansfield, D. Mauzey, R. Nguyen, and M. Vorenkamp, "A Quasi-Periodic Linear Feeder for the Impurity Granular Injection on DIII-D", *IEEE Trans. Plasma Sci.* 46 (2018) 1120.
- 11. G.Z. Zuo, J.S. Hu, Y.W. Yu, Z. Sun, R. Maingi, H.D. Zhuang, X.C. Meng, W. Xu, D.K. Mansfield, K. Tritz, B.Zhang, C.Y. Xie, M. Huang, J.H.Wu, J.G. Li and the EAST Team, "Reduction of hydrogen content in deuterium plasma with mixed graphite and tungsten divertors in EAST", *Fusion Eng. Design* **131** (2018) 41.

- 12. W. Xu, J.S. Hu, G.Z. Zuo, Z. Sun, R. Lunsford, X.C. Meng, M. Huang, "A new developed inbetween shots lithium evaporation coating system for improving plasma performance in EAST", *Fusion Eng. Design* **133** (2018) 142.
- 13. R. Rizkallah , D. Andruczyk , A. Shone, D. Johnson, Z. Jeckell, S. Marcinko, Z. Song, D. Curreli, F. Bedoya, A. Kapat, J. P. Allain, M. Christenson, M. Szott, S. Stemmley, H. Sandefur, D. N. Ruzic, R. Maingi, J. Hu, G. Zuo, and J. Schmitt, "Latest results from the Hybrid device for research and applications (HIDRA)", *IEEE Trans. On Plasma Sci.* 46 (2018) 2685.
- 14. Z. Sun, J.K. Baldwin, Z. Wang, J.S. Hu, R. Maingi, C. Romero-Talamas, D.M. Oschwald, "Initial results and designs of dual-filter and plenoptic imaging for high-temperature plasmas", *Rev. Sci. Instrum.* **89** (2018) 10E112.
- 15. P. Chu, T.W. Bradley, and Z. Wang, "Measurement of incandescent microparticle acceleration using stereoscopic imaging", *Rev. Sci. Instrum.* **89** (2018) 10K101.
- 16. J. Sun, L. Liu, Z. Sun, M. Li, and D. Wang, "Numerical simulation of Li pellet ablation in the H-mode pedestal region", *Fusion Eng. Design* **136** (2018) 834.
- 17. W. Xu, Z. Sun, J.S. Hu, G.Z. Zuo, R. Maingi, D. Mansfield, M. Huang, X. C. Meng, J.G. Li, A. Diallo, R. Lunsford, T. Osborne, K. Tritz, and EAST team, "Real-time reduction of tungsten impurity influx using lithium powder injection in EAST", *Fusion Eng. Design* **137** (2018) 202.
- 18. A. Nagy, A. Bortolon, D.M. Mauzey, E. Wolfe, E.P. Gilson, R. Lunsford, R. Maingi, D.K. Mansfield, R. Nazikian, A.L. Roquemore, "A Multi-Species Powder Dropper For Magnetic Fusion Applications", *Rev. Sci. Instrum.* **89** (2018) 10K121.
- 19. G.Z. Zuo, J.S. Hu, R. Maingi, Z. Sun, Q. X. Yang, M. Huang, X. C. Meng, W. Xu, X.Z. Gong, K. Tritz, A. Diallo, R. Lunsford, J.G. Li and EAST team, "Results from an improved flowing liquid lithium limiter with increased flow uniformity in high power plasmas in EAST", *Nucl. Fusion* **59** (2019) 016009.
- R. Lunsford, J.S. Hu, Z. Sun, R. Maingi, D. K.Mansfield, W. Xu, G.Z. Zuo, M. Huang, A. Diallo, T. Osborne, K. Tritz, J. Canik, X. C. Meng, Q. Zang, X. Z. Gong, B.N. Wan, J.G. Li, and the EAST team, "ELM Frequency Enhancement and Discharge Modification through Lithium Granule Injection into EAST H-modes", *Nucl. Fusion* 58 (2018) 126021.
- 21. G.Z. Zuo, J. Ren, X.C. Meng, Z. Sun, W. Xu, M. Huang, J.S. Hu and J.G. Li, "Investigation of wettability of Li on 316L SS surface and interfacial interactions for fusion device", *Fusion Eng. Design* **137** (2018) 420.
- 22. M. Szott, Z. Wang, and D. Ruzic, "Reconstruction and analysis of exploding wire particle trajectories via automatic calibration of stereo images", *Rev. Sci. Instrum.* **89** (2018) 10K118.
- X. Liu, V. Naulin, J. Xu, G.Z. Deng, J. Rasmussen, J.B. Liu, A. Nielsen, R. Goldston, R. Maingi, Y. Liu, G.S. Xu, L. Wang, J.G. Li, "Statistical study of particle flux footprint widths with tungsten divertor in EAST", *Plasma Phys. Control. Fusion* 61 (2019) 045001.
- 24. A. Bortolon, V. Rohde, R. Dux, R. Maingi, E. Wolfrum, A. Nagy, A. Herrmann, R. Lunsford, R. McDermott, A. Kallenbach, R. Neu, D.K. Mansfield, R. Nazikian and the ASDEX-Upgrade team, "Real-time wall conditioning by controlled injection of boron and boron nitride powder in full tungsten wall ASDEX-Upgrade", *Nucl. Mater. Energy* 19 (2019) 384.
- 25. Z. Sun, R. Maingi, J.S. Hu, W. Xu, G.Z. Zuo, Y.W. Yu, C.R. Wu, M. Huang, X.C. Meng, L. Zhang, L. Wang, S.T. Mao, F. Ding, D.K. Mansfield, J. Canik, R. Lunsford, A. Bortolon, X.Z. Gong and EAST team, "Real Time Wall Conditioning for Long Pulse Plasma by Using Lithium Powder Injection in EAST with Tungsten Divertor", Nucl. Mater. Energy 19 (2019) 124.

- 26. J.S. Hu, G.Z. Zuo, R. Maingi, Z. Sun, K. Tritz, W. Xu, Q. X. Yang, D. Andruczyk, M. Huang, X. C. Meng, X.Z. Gong, D. N. Ruzic, M.J. Ni, B.N. Wan, J.G. Li and EAST team, "Experiments of continuously and stably flowing lithium limiter in EAST towards a solution for the power exhaust of future fusion devices", *Nucl. Mater. Energy* 18 (2019) 99.
- 27. X.C. Meng, C. Xu, H. Q. Deng, J. S. Hu, G.Z. Zuo, M. Huang, K. Tritz, D. Andruczyk, Z. Sun, W. Xu, Y. Z. Qian, J. J. Huang, X. Gao, B. Yu, J. G. Li, "Corrosion characteristics of copper in static liquid lithium under high vacuum", *J. Nucl. Mater.* **513** (2019) 282.
- 28. Y. L. Li, G. S. Xu, K. Tritz, X. Lin, H. Liu, Y. Chen, S. Li, F. Yang, Z. W. Wu, L. Wang, H. Lan, X. L. Li, W. Zhang, G. H. Hu, "Upgrade of the multi-energy soft x-ray diagnostic system for studies of ELM dynamics in the EAST tokamak," *Fusion Eng. Design* **137** (2018) 414.
- 29. J.D. Lore, R.S. Wilcox, J.M. Canik, L. Wang, G.S. Xu, and R. Maingi, "Optimization of pumping performance in the EAST upgraded divertor", *Plasma Phys. Control. Fusion* **61** (2019) 065001.
- 30. Z. Wang, M. Hoffbauer, E. Hollmann, Z. Sun, Y. Wang, N. Eidietis, J.S. Hu, Jiansheng; R. Maingi, J. Menard, X. Xu, "Hollow pellet injection for magnetic fusion", *Nucl. Fusion* **59** (2019).
- 31. X. Gong, A. M. Garofalo, J. Huang, J. Qian, C.T. Holcomb, A. Ekedah, R. Maingi, E. Li, L. Zeng, B. Zhang, J. Chen, M. Wu, H. Du, M. Li, X. Zhu, Y. Sun, G. Xu, Q. Zang, L. Wang, L. Zhang, H. Liu, B. Lyu, P. Sun, S. Ding, X. Zhang, F. Liu, Y. Zhao, B. Xiao, J. Hu, C. Hu, L. Hu, J. Li, B. Wan and the EAST team, "Integrated operation of steady-state long pulse H-mode in EAST", *Nucl. Fusion* **59** (2019).